ROISD: **R**IS and **O**-RAN Assisted **I**ntelligent **S**ensing for UAV **D**etection

Xiaochan Xue*, Shucheng Yu†, Saurabh Parkar*, Yao Zheng*
*Department of Electrical and Computer Engineering, University of Hawai'i at Mānoa, HI 96822, USA
†Department of Graduate Computer Science and Engineering, Yeshiva University, NY 10033, USA
Email: {xxue,sparkar,yaozheng}@hawaii.edu, shucheng.yu@yu.edu

***Abstract*—The growing proliferation of unmanned aerial vehicles (UAVs) has intensified security concerns, particularly from high-speed unauthorized flights in restricted airspaces. Conventional detection methods based on radar, acoustic, vision, and RF sensing, facing inherent limitations in cost, scalability, and environmental robustness, and lack the coordination necessary for wide-area coverage against fast maneuvering threats. To address these limitations, we propose a RIS and O-RAN assisted framework within the Integrated Sensing and Communication (ISAC) paradigm, adapted for the 3.7 GHz Citizens Broadband Radio Service (CBRS) band. The system leverages programmable RIS to improve signal observability and employs O-RAN distributed intelligence for multi-stage UAV detection. A composite OFDM–FMCW waveform provides high-resolution range–Doppler sensing, and a GRU-based predictive controller enables low-latency RIS adaptation. Experimental results, conducted under realistic deployment constraints, demonstrate that a single sensing node achieves reliable detection sufficient to trigger stage transitions. These results confirm the feasibility of integrating RIS and O-RAN for high-speed UAV sensing.**

***Index Terms*—UAV detection, Open Radio Access Network (O-RAN), 6G, beyond 5G, Reconfigurable Intelligent Surfaces (RISs), multi-beam design, Integrated sensing and communication (ISAC), machine learning, intelligent controller, adaptive coordination, resource management.**

I. Introduction

The rapid proliferation of Unmanned Aerial Vehicles (UAVs) across civilian, commercial, and military sectors has transformed modern applications, enabling new capabilities in aerial surveillance, package delivery, environmental monitoring, and disaster response. However, this growth also introduces critical security concerns. Unauthorized or malicious UAVs intruding into restricted airspaces near airports, government facilities, or critical infrastructure can cause severe disruptions, including flight cancellations, security breaches, and privacy violations. High-speed UAVs further intensify these risks, as their mobility and unpredictable trajectories can overwhelm conventional monitoring systems and hinder timely response. Consequently, developing reliable, timely, and scalable UAV detection systems has become a central research priority in next-generation wireless networks.

Despite progress in UAV detection, all existing approaches face fundamental limitations that hinder robust and scalable deployment [1, 2]. Radar systems provide accurate range and velocity estimates but demand significant infrastructure and incur high operational costs. Acoustic and vision methods are highly sensitive to environmental conditions such as noise, weather, and lighting. Radio frequency (RF) approaches suffer from line-of-sight restrictions and limited adaptability to evolving UAV technologies. Most critically, these approaches operate in isolation and lack the coordination necessary for wide-area coverage, underscoring the urgent need for scalable, adaptive, and collaborative detection solutions.

Two emerging technologies offer promising opportunities to address these challenges. *Reconfigurable Intelligent Surfaces* (RIS) enable programmable manipulation of electromagnetic propagation through reflection, refraction, and scattering, extending coverage, and mitigating line-of-sight (LoS) constraints. Their flexible, actively reconfigurable control of wavefronts allows dynamic beam steering and adaptive coverage shaping, providing cost-effective deployment while maintaining resilience against evolving threats. *Open Radio Access Networks* (O-RAN) provide a complementary foundation through an open, disaggregated, and AI-native architecture that enables distributed intelligence and inter-node collaboration, supporting hierarchical detection from coarse surveillance to fine-grained localization.

The convergence of RIS and O-RAN naturally points toward *Integrated Sensing and Communication* (ISAC) as the next stage of wireless evolution, enabling spectrum and infrastructure sharing between communication and sensing. However, realizing RIS-assisted UAV detection within ISAC frameworks requires moving beyond communication-centric designs. Traditional Orthogonal Frequency-Division Multiplexing (OFDM) based RIS implementations lack the range–Doppler resolution and channel tracking capabilities required for reliable moving target detection. Advanced waveform designs, such as composition of OFDM and Frequency Modulated Continuous Wave (FMCW) signals and modified OFDM variants, are needed to overcome RIS hardware constraints and enable dual-purpose operation for both communication and UAV sensing under dynamic conditions.

In this work, we present a RIS and O-RAN assisted ISAC framework for UAV detection and trajectory tracking in the Citizens Broadband Radio Service (CBRS) band at 3.7 GHz. The CBRS spectrum provides a good balance between coverage and sensing resolution, and supports flexible spectrum access under FCC regulation. Our system combines RIS-based signal control with O-RAN-enabled distributed processing to enable scalable and adaptive sensing. A state-machine-guided detection strategy allows the system to switch between wide-

area scanning and focused tracking, depending on UAV motion and detection confidence. With real-time coordination and prediction integrated into the O-RAN control process, the system achieves stable performance across different flight patterns and sensing conditions. Our main contributions are summarized as follows:

- We introduce a RIS and O-RAN assisted ISAC framework that addresses the limitations of current UAV detection technologies through adaptive sensing, predictive control, and distributed coordination.
- We develop a hierarchical detection scheme with state-machine guidance and GRU-based trajectory prediction, enabling dynamic transitions from wide-area exploration to focused tracking.
- We implement cross-layer resource management under spectrum-sharing constraints, leveraging O-RAN's Near-RT and Non-RT control architecture to support scalable and low-latency RIS reconfiguration.
- We validate the proposed framework through system-level simulations, demonstrating significant improvements in detection accuracy, responsiveness, and robustness under diverse UAV dynamics.

The remainder of this paper is organized as follows. Section II reviews related work. Section III introduces the technical background. Section IV presents the detection scheme, followed by results in Section V. Section VI concludes the paper and provides future direction.

II. Related Work

This section reviews prior work in four key areas: UAV detection technologies, composite waveform designs for ISAC, RIS-assisted sensing, and O-RAN for distributed intelligence. We highlight the gaps that motivate our integrated approach.

Traditional UAV detection relies on single-sensor modalities, each with distinct strengths and limitations [1, 2]. Acoustic methods [3–7] exploit propulsion noise and can operate in non-line-of-sight (NLOS), however, the performance degrades under ambient noise, wind, and adverse weather. Vision-based systems [8–13] use deep learning but remain vulnerable to low illumination, occlusion, and limited range. RF-based detection [14–18] passively monitors control links; However, the performance declines as autonomous UAVs reduce RF dependence or fly RF-silent. Radar provides precise range and velocity via Doppler, although dedicated infrastructure and heavy processing hinder large-scale deployment [19–21]. Multi-modal fusion combines complementary cues and improves robustness [22–24]; however, most implementations remain isolated, single-node designs without distributed coordination, which is problematic for fast UAVs whose rapid maneuvers demand high temporal resolution and collaborative multi-node tracking.

Reconfigurable Intelligent Surfaces (RIS) have received growing attention in wireless communications for their ability to enable programmable beam steering, enhance coverage, and manage interference [25]. A RIS consists of an array of controllable tiles that adjust the phase of incoming signals to form desired beam patterns and reshape the wireless environment. In addition to traditional communication functions, recent studies have explored using RIS for sensing tasks such as target localization, angle-of-arrival (AoA) estimation, and channel state information enhancement [8, 26]. However, standard passive RIS hardware remains limited in functionality. Individual tiles typically lack circuitry for demodulation, waveform-specific filtering, or adaptive control. Although active RIS designs can support these features, they often introduce considerable power and computational overhead, which challenges scalable deployment. Current RIS implementations are unable to separate sensing and communication waveforms at the surface level without interference.

To address these limitations, ISAC waveform design provides multiple methods to dual functionality. Modified OFDM variants embed sensing features into communication resources so that a single signal serves both roles [27, 28]. A complementary approach is the composite OFDM–FMCW signal, which combines an FMCW component with OFDM to couple fine range–Doppler sensing with data delivery. Recent work demonstrates thefeasibility with favorable bandwidth efficiency and low implementation overhead [29]. These approaches enable dual-purpose RIS operation without additional hardware [30], allowing tiles or time slots to be assigned to sensing or communication with separation handled in baseband. Meanwhile, hardware advances are pushing RIS beyond purely passive designs: relay-type RIS [31, 32] and amplifying-and-filtering RIS (AF-RIS) [33] incorporate simple analog modules (e.g., amplifiers, bandpass filters, low-power processors) in selected tiles. These enhancements improve local signal quality, reduce latency, and support limited edge processing even without full base-station coordination. As a result, RIS is evolving from a passive reflector into a low-power, intelligent node that can actively contribute to ISAC operations in future wireless networks.

O-RAN provides an open, disaggregated, AI-native architecture that enables distributed intelligence and real-time coordination [34]. With RAN Intelligent Controllers (RIC) operating at near real-time (Near-RT) and non real-time (Non-RT) timescales, O-RAN can manage short and long term data to adaptively control RIS across heterogeneous cells. Near-RT RICs run xApps that adjust RIS phase shifts, beam directions, and scheduling hooks in response to channel dynamics, user mobility, and network load [35–38], while Non-RT RICs perform policy optimization, model training, and analytics that guide Near-RT decisions [39, 40]. This hierarchical control loop supports continuous RIS adaptation, balancing immediate performance (e.g., throughput, latency) with longer-term goals (e.g., energy, reliability). ML-based applications on the RIC further enhance flexibility by jointly optimizing throughput, fairness, and security using real-time and historical data. Studies indicate that software-driven RIS management enables user tracking, beam steering, and resource allocation, laying the groundwork for scalable, cooperative UAV sensing with RIS-enhanced propagation.

Integration of RIS and O-RAN within ISAC frameworks has

received limited attention. Most prior work assumes idealized RIS behavior and simplified sensing tasks, without addressing hardware constraints or high mobility scenarios requiring fine range-Doppler resolution. Shared spectrum environments such as the CBRS band also remain underexplored, despite their practical importance. Existing UAV detection approaches lack distributed coordination for wide-area surveillance, and RIS hardware limits are rarely considered in waveform and functional design. The potential of O-RAN for collaborative sensing is largely unexplored, as most studies remain communication-centric. Moreover, comprehensive frameworks that jointly address waveform design, resource allocation, and hierarchical detection under spectrum sharing are still absent.

III. System Model

In this section, we establish the system model (Fig. 1) for RIS-assisted UAV detection under the ISAC framework. The transmitted signal is composed of a composite ISAC waveform, where the FMCW component serves the sensing functionality while coexisting with communication signals such as OFDM. We focus on the FMCW-based sensing process, which enables range, angle, and velocity estimation of UAV targets when reflected by the RIS. The following subsections describe the measurement model and link budget analysis that characterize the received signal and its propagation dynamics.

A. RIS-Assisted FMCW Sensing and Measurement

Relative Position: At each discrete sensing time slot t_k, the RIS-assisted O-RAN system utilizes FMCW signaling to perform UAV detection and characterization. FMCW waveforms enable simultaneous range and velocity estimation by analyzing the beat frequency and Doppler shift of reflected signals. Let $\mathbf{p}(t_k) \in \mathbb{R}^3$ and $\mathbf{v}(t_k) \in \mathbb{R}^3$ denote the position and velocity vectors of the UAV at time t_k, and let $\mathbf{p}_{\text{RIS}} \in \mathbb{R}^3$ denote the known position of the RIS. The relative position vector is defined as

$$\mathbf{r}(t_k) = \mathbf{p}(t_k) - \mathbf{p}_{\text{RIS}}, \tag{1}$$

where $\mathbf{r}(t_k) = [r_E(t_k), r_N(t_k), r_U(t_k)]^T$ represents the relative position in the 3D East-North-Up (ENU) coordinate system.

Distance: The FMCW-based measurements are obtained as follows. The range is estimated from the beat frequency as

$$d_k = \frac{c}{2B} f_{b,k}, \tag{2}$$

where $f_{b,k}$ is the dechirped beat frequency, B is the sweep bandwidth, and c is the speed of light. Here, $f_{b,k}$ directly reflects the round-trip propagation delay and serves as the key intermediate observable that maps the time delay into a measurable range.

Angles: The spatial bearing of the UAV relative to the RIS is characterized by the azimuth angle

$$\theta_k = \arctan 2(r_E(t_k), r_N(t_k)), \tag{3}$$

and the elevation angle

$$\phi_k = \arctan 2\left(r_U(t_k),\ \sqrt{r_E^2(t_k) + r_N^2(t_k)}\right). \tag{4}$$

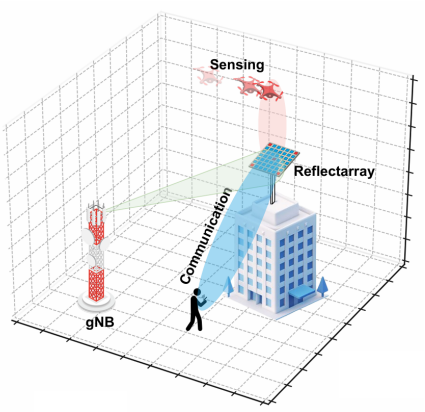

Figure 1. Illustration of a RIS-assisted ISAC system for UAV detection. The gNB communicates with the UE through a reflectarray while leveraging the reflected waveform for UAV sensing.

The radial velocity, corresponding to the UAV's motion along the LoS direction, is expressed as

$$v_{r,k} = \frac{\mathbf{r}(t_k)^T \mathbf{v}(t_k)}{\|\mathbf{r}(t_k)\|_2}, \tag{5}$$

where the subscript r denotes the radial component, and is directly related to the Doppler shift via $f_{D,k} = \frac{2v_{r,k}}{\lambda}$, where λ is the carrier wavelength.

B. Link Budget and Path Loss

To account for propagation effects, we adopt a radar link budget formulation. The received power in the monostatic FMCW setting is

$$P_{r,k} = \frac{P_t G_t G_r \lambda^2 \sigma_k}{(4\pi)^3 d_k^4 L_{\text{sys}}}, \tag{6}$$

where P_t is the transmit power, G_t and G_r are the antenna gains, σ_k is the radar cross section (RCS), and L_{sys} captures system losses. When a RIS is configured to assist the sensing process, the cascaded propagation via the transmitter–RIS–UAV–receiver path introduces an additional gain factor G_{RIS}, which depends on the number of reflecting tiles, their phase alignment, and reflection efficiency. The per-slot signal-to-noise ratio is then

$$\text{SNR}_k = \frac{P_{r,k} G_{\text{int}}}{k_B T_0 F_N B}, \tag{7}$$

where G_{int} denotes the coherent integration gain, k_B is Boltzmann's constant, T_0 the noise temperature, F_N the receiver noise figure, and B the sweep bandwidth. This SNR_k directly influences the estimation accuracy of range, angle, and velocity, and its dependence is embedded in the measurement noise covariance matrix. The complete measurement vector at time slot k is therefore expressed as

$$\mathbf{z}_k = \left[d_k,\ \theta_k,\ \phi_k,\ v_{r,k},\ \text{SNR}_k\right]^T + \mathbf{n}_k, \tag{8}$$

where $\mathbf{n}_k \sim \mathcal{N}(\mathbf{0}, \mathbf{R}_k)$ represents estimation errors due to noise, clutter, and multipath. The covariance matrix $\mathbf{R}_k$ is parameterized as a decreasing function of SNR_k, ensuring consistency with estimation theory.

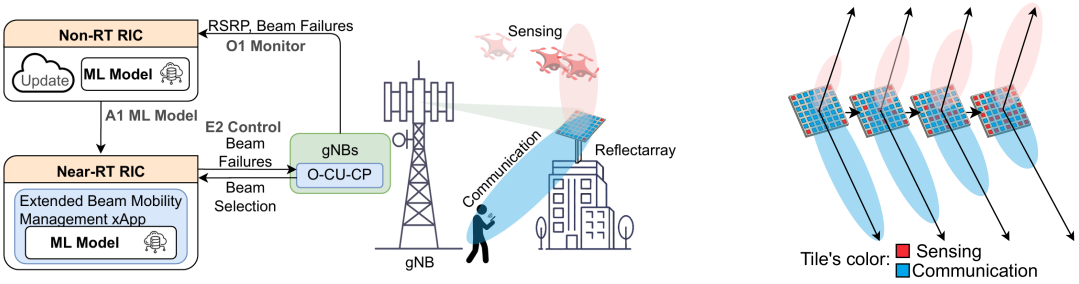

(a) (b)

Figure 2. Illustration of O-RAN based RIS configuration and resource allocation. (a) O-RAN based RIS initial configuration via ML control and beam management. (b) Adaptive tile level coordination for dynamic RIS resource allocation across sensing and communication tasks.

C. UAV Detection

Successful radar detection of UAVs depends on their electromagnetic visibility, commonly characterized by the radar cross section (RCS). The RCS is the effective area that reflects incident energy back to the radar and is defined in [41] as:

$$\sigma = \lim_{R\to\infty} 4\pi R^2 \frac{|E_s|^2}{|E_i|^2} \tag{9}$$

Where: σ is expressed in m^2 or logarithmically in dBsm, R is the distance in meters, E_i is the incident electric field strength, and E_s is the scattered electric field strength. Commercial UAVs exhibit low and frequency dependent RCS in the CBRS band, typically ranging from about -24 to -5 dBsm depending on aspect angle and materials (e.g., plastics, carbon fiber composites). The dominant scattering contributions arise mainly from metallic components such as batteries, printed circuit boards, and motors, whose effective reflectivity varies significantly with the aspect angle between the UAV and the radar line-of-sight [42–44].

Furthermore, the RCS is also dependent on factors such as the transmitted power P_t, wavelength of operating frequency λ, the transmit gain G_t and the receive gain G_r as shown in Eq. 6. Based on these Eq. 6 and Eq. 9, the target RCS can be derived based on the received power and vice versa, enabling the setup of SNR thresholds for accurate detection of UAVs. Utilizing a noise removal or clutter elimination algorithm such as covariance-based filtering, extensive cancellation algorithms (ECA), or their adaptive variants helps to suppress static reflections and direct-path interference before thresholding. The detection process can then be performed by applying a SNR based thresholding besides a constant false-alarm rate (CFAR) on the processed range–Doppler map [44–47].

IV. Scheme

The detection, identification, and tracking of fast UAVs rely on collaborative sensing, which requires continuous coordination among multiple geographically distributed gNBs to establish an adaptive UAV sensing corridor while simultaneously ensuring communication services. In this section, we propose a resource aware scheme under the O-RAN framework that leverages multiple RIS-assisted sensing to collaboratively detect high-speed, maneuverable low altitude UAVs as shown in Fig. 2. Through RIS configuration and waveform adaptation, the proposed approach achieves efficient sensing while preserving reliable communication for user equipment (UE).

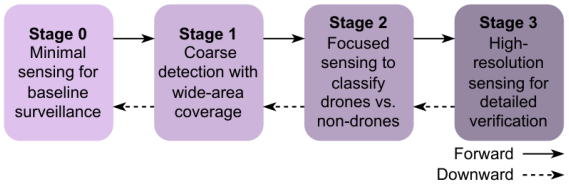

Figure 3. State machine for adaptive UAV sensing. Equipped with backward transitions enabled for re-verification or uncertainty handling.

A. Multi-Stage State Machine for Adaptive Detection

The core of our solution is a multi-stage state machine $\mathcal{S} = \{S_0, S_1, S_2, S_3\}$ as shown in Fig. 3, which provides adaptive logic for RIS beam scheduling and waveform adaptation. Each state corresponds to progressively refined detection objectives with increasing sensing and resource demands:

Stage 0 (Idle): Continuous wide-angle surveillance with minimal resource usage, serving as the baseline monitoring mode to ensure coverage of the sensing region.

Stage 1 (Initial Detection): Coarse UAV detection through low-resolution FMCW sweeps, enabling rapid identification of potential targets across a broad area.

Stage 2 (Classification): Target-focused sensing with refined angle and velocity estimation, used to discriminate UAVs from birds, ground clutter, or other moving objects.

Stage 3 (Identification): High-resolution sensing with narrow beams and enhanced SNR, providing precise characterization of UAV features such as trajectory, size, and motion dynamics.

State transitions are driven by detection confidence γ_i, configurable thresholds τ_i, and real-time resource availability:

$$P(S_i \to S_j) = \begin{cases} f(\gamma_i, \tau_i, \mathbf{c}_{\text{avail}}, Q_i, \mathbf{z}_k), & \text{if } j = i+1, \\ g(\gamma_i, t_{\text{timeout}}, Q_i, \epsilon_{\text{cov}}), & \text{if } j < i, \\ 0, & \text{otherwise} \end{cases} \tag{10}$$

where γ_i is the detection confidence at stage S_i (derived from accumulated SNR and track consistency), τ_i is the transition threshold for advancing from S_i to S_{i+1}, $\mathbf{c}_{\text{avail}}$ denotes the set of RIS configurations available under current resource and

QoS constraints, Q_i is the communication QoS metric (e.g., latency, throughput), $\mathbf{z}_k$ is the FMCW measurement vector in eq. (8), and ϵ_{cov} is a constraint ensuring the integrity of the collaborative sensing. The forward transition function $f(\cdot)$ promotes to the next stage when detection confidence exceeds the threshold and sufficient resources are available. The downward transition $g(\cdot)$ reverts to a previous stage due to timeout, low confidence, or QoS violations.

B. RIS Configuration Space

We define a discrete RIS configuration space $\mathcal{C} = \{\mathbf{c}_1, \mathbf{c}_2, \ldots, \mathbf{c}_M\}$ where each configuration $\mathbf{c}_i$ includes the programmable phase shift matrix $\mathbf{\Phi}_i = [\phi_{mn}]_{N\times N}$ for the $N \times N$ RIS tiles, beam pattern descriptor $\mathbf{b}_i = [\theta_{\text{center}}, \phi_{\text{center}}, \Delta\theta, \Delta\phi]$ specifying beam center and beamwidth, and sensing power allocation $P_{\text{sens},i}$ for the FMCW component, represented as $\mathbf{c}_i = \{\mathbf{\Phi}_i, \mathbf{b}_i, P_{\text{sens},i}\}$. The subset of available configurations $\mathbf{c}_{\text{avail}} \subseteq \mathcal{C}$ appearing in (10) is determined dynamically based on hardware actuation limits and communication QoS requirements. The configuration space is strategically partitioned according to detection stages:

- $\mathcal{C}_{S_0}$ uses minimal phase control for continuous surveillance with ultra-wide beams;
- $\mathcal{C}_{S_1}$ uses coarse phase granularity for wide-area detection with broad beams;
- $\mathcal{C}_{S_2}$ employs medium granularity for focused classification with medium beams;
- $\mathcal{C}_{S_3}$ applies fine granularity for high-precision identification with narrow beams.

This partitioning enables efficient resource allocation while maintaining sensing integrity. The intersection $\mathcal{C}_{S_{i+1}} \cap \mathbf{c}_{\text{avail}}$ represents the set of feasible configurations for transitioning to the next detection stage.

C. GRU-Based Predictive RIS Configuration

To support fast and proactive RIS reconfiguration, we design a Gated Recurrent Unit (GRU)–based model that predicts the next RIS configuration using state machine status, FMCW measurements, and system history. GRUs are selected for their efficiency and ability to learn patterns over time while meeting the sub-100,ms response requirement of the Near-RT RIC.

$$\hat{\mathbf{c}}[k+1] = \text{GRU}(\mathbf{c}[k-W:k], \mathbf{s}[k], \mathbf{z}[k], \gamma[k]; \boldsymbol{\theta}_{\text{GRU}}) \quad (11)$$

where $\hat{\mathbf{c}}[k+1]$ is the predicted RIS configuration for the next time slot, $\mathbf{c}[k-W:k]$ is the sliding-window history of configurations over W slots, $\mathbf{s}[k] \in \{S_0, S_1, S_2, S_3\}$ is the current state machine stage, $\mathbf{z}[k]$ is the current FMCW measurement vector, $\gamma[k]$ is the detection confidence at time k, and $\boldsymbol{\theta}_{\text{GRU}}$ represents trainable GRU parameters. The GRU architecture processes temporal sequences to predict both the next optimal beam direction and the required phase shift matrix $\hat{\mathbf{\Phi}}_{k+1}$. Training emphasizes diverse operational scenarios including varied weather conditions (rain, fog affecting path loss), multipath-rich urban environments with RCS variations, and high-speed maneuvers to ensure robust generalization across real-world drone behaviors.

D. O-RAN Integration Architecture

The predictive RIS control framework is integrated into the O-RAN architecture through three standardized interfaces that coordinate near-real-time inference, long-term policy updates, and hardware control.

Near-RT RIC (xApp): The GRU-based controller operates as an xApp in the Near-RT RIC, supporting fast adaptation with control loops on the order of 100 ms. It receives FMCW measurement vectors from the DU via the E2 interface, along with the current state $\mathbf{s}[k]$, detection confidence $\gamma[k]$, and QoS metrics Q_i. Based on this information, the xApp performs inference to predict the next RIS configuration $\hat{\mathbf{c}}[k+1]$ and issues control decisions.

Non-RT RIC (Policy and Training): Long-term model updates and system policies are managed by the Non-RT RIC via the A1 interface. This includes parameter tuning for the predictive model $\boldsymbol{\theta}_{\text{GRU}}$, configuration thresholds $\{\tau_0, \tau_1, \tau_2, \tau_3\}$, and balancing strategies between sensing and communication resource usage.

O1 Interface (Execution): The predicted configuration $\hat{\mathbf{c}}[k+1]$ is applied through the O1 interface using NETCONF/YANG protocols, translating into RIS phase shifts $\mathbf{\Phi}_{k+1}$, waveform parameters such as bandwidth B and chirp duration, and power allocation directives.

This architecture supports closed-loop control by combining real-time sensing with longer-term optimization. It enables intelligent RIS adaptation with minimal latency, scalable coordination across network elements, and seamless integration of ML-based decision-making into O-RAN.

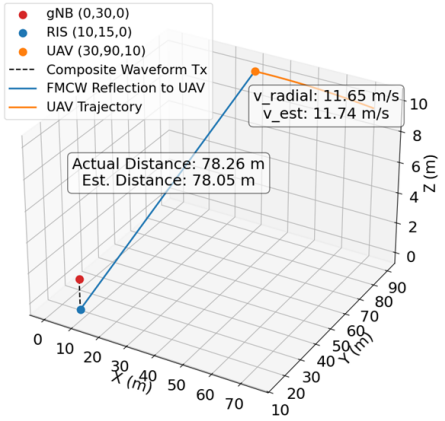

Figure 4. UAV trajectory in a 3D East-North-Up (ENU) coordinate system.

V. Evaluation

This section evaluates the proposed RIS and O-RAN enabled UAV detection framework through simulation-based experiments that emulate realistic deployment conditions. We first describe the experimental setup, then demonstrate the multi-stage detection process, and finally validate the GRU-based trajectory prediction for adaptive beam control.

A. Experimental Setup

Fig. 4 shows a gNB is placed at the origin at a height of 30 m, with a RIS deployed 18 m away at a height of 15 m.

Signal Processing and Angle Estimation: The azimuth θ_k and elevation ϕ_k are estimated with 2D Multiple Signal Classification (MUSIC). This algorithm exploits the orthogonality between the array steering vectors corresponding to the true directions of arrival (DoA) and the noise subspace of the received signal covariance matrix. By scanning a 2D azimuth–elevation grid and evaluating the MUSIC pseudospectrum yields sharp peaks at the actual DoAs, enabling super-resolution beyond conventional beamforming.

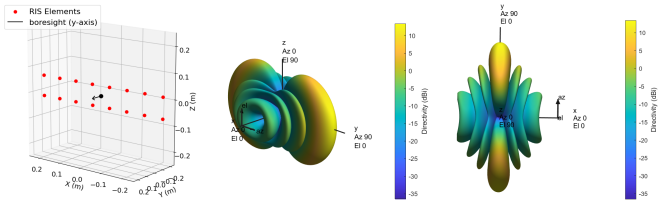

(a) (b) (c)

Figure 5. RIS array configuration and directivity patterns. (a) An 8×2 RIS array in 3D. (b) and (c) show simulated directivity patterns for different azimuth/elevation combinations, illustrating beamforming capabilities.

UAV and Waveform Modeling: The RIS is modeled as a hybrid relay-type RIS capable of limited telemetry and local signal processing, such as estimating the angle of arrival (AoA) at the RIS itself. The UAV is modeled as a moving target with a mean RCS of -14 dBsm ($0.04\ m^2$), providing sufficient detection margin for small to medium-sized drones according to values specified in [44]. Uniform acceleration is applied in 3D space to emulate realistic flight trajectories.

A composite OFDM–FMCW waveform is transmitted at 3.7 GHz under free-space path loss. The FMCW component is filtered and reflected by the RIS in the ENU plane for UAV detection. The 8×2 RIS lies in the x–z plane with boresight along $+y$, providing broad coverage for Stage 0 (Fig. 5a). Each tile is spaced at half the carrier wavelength, satisfying the Nyquist criterion to avoid spatial aliasing and grating lobes. The resulting array directivity patterns are illustrated in Fig. 5b and 5c. The horizontal aperture provides fine angular resolution in azimuth, while the vertical extension enhances elevation sensitivity for discriminating vertically separated targets. Despite its compact size, the 8×2 configuration offers a favorable trade-off between angular resolution, hardware complexity, and computational cost.

B. Multi-Stage Detection

The proposed framework operates through four stages, each with increasing sensing resolution and resource allocation, as defined in the state machine (Section IV).

As shown in Table I, the FMCW waveform uses a 50 MHz sweep bandwidth and 11 μs sweep duration, supporting detection ranges up to 300 m and speeds up to 350 km/h, covering typical commercial and survey-class UAV operations. A coherent processing interval (CPI) of 64 sweeps over 0.705 ms provides the temporal resolution for Doppler-based velocity estimation. This sets up the initial surveillance for

Table I
FMCW RADAR SPECIFICATIONS

Parameter	Value
Operating Frequency (F_c)	3.7 GHz
Sweep Duration (T)	11 μs
Sweep Bandwidth (B)	50 MHz
Range Resolution	3 m
Max Target Range ($R_{\max}$)	300 m
Max Target Speed	350 km/h

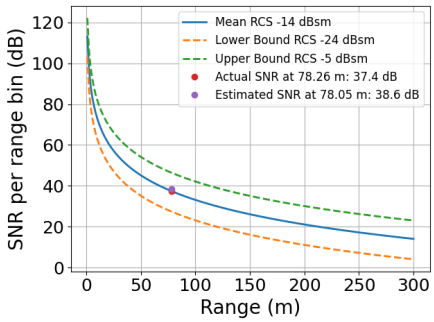

Figure 6. SNR threshold-based detection for UAV.

target detection in **Stage 0**. The sweeps are transmitted in an ENU setting and cover a wide area for coarse target sensing in the environment for **Stage 1**. Upon detection, the system increases sensing priority (power and, when permitted, sweep bandwidth) and applies SNR threshold-based identification per CPI for UAV classification. The incident angles (θ_k, ϕ_k) and radial velocity $v_{r,k}$ *are* estimated to drive the RIS steering state machine in **Stage 2**. For thresholding, we use an upper RCS bound of -5 dBsm ($0.32\ \mathrm{m}^2$) to represent favorable line-of-sight aspects and a lower bound of -24 dBsm ($0.004\ \mathrm{m}^2$) for unfavorable orientations. Subsequent CPIs then operate with the increased sweep bandwidth to refine 3D tracking. In **Stage 3**, selected RIS tiles are steered toward the target for fine tracking, while the remaining tiles continue wide-area scanning to discover new targets.

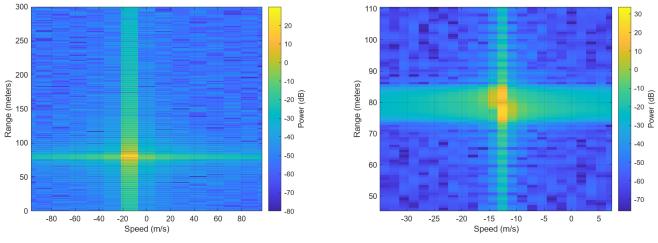

(a) (b)

Figure 7. Comparison of velocity estimation: (a) raw Doppler response from dataset; (b) post-processed result showing enhanced target visibility.

The expected SNR bounds over the coverage area for UAV classification are shown in Fig. 6. Here, our simulated UAV is detected with a SNR of 38.6 dB with a difference of 1.2 dB as compared to the expected SNR of 37.4 dB. This difference is likely due to the slight mismatch in range estimation. The range–velocity map for a single CPI is shown in Fig. 7a. Over a 2 ms CPI duration, the target response

appears smeared around the true range bin (actual: 78.26 m, estimated: 79.07 m) and radial velocity (actual: 11.65 m/s, estimated: 11.74 m/s). As responses from multiple CPIs are accumulated, the object movement becomes clearer: the range map shows concentration between 78–88 m and the radial velocity clusters around –11 to –14 m/s (negative indicates the target is moving away from the RIS), capturing the simulated acceleration over a 90 ms interval as illustrated in Fig. 7b.

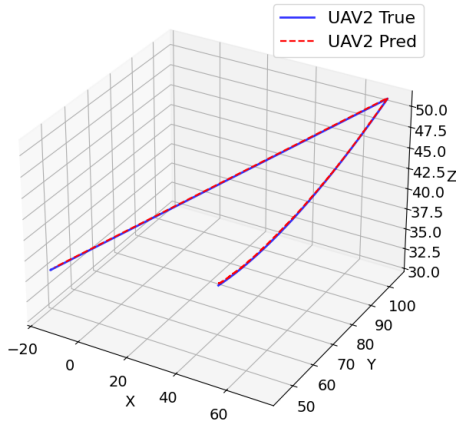

Figure 8. Groud truth and predicted trajectory of UAV2.

C. GRU-Based Prediction

The near-RT RIC offers cloud-native control with 1 ms–1 s response, enabling real-time coordination of RIS for sensing. To predict motion for beam steering, we adopt a GRU model. After each sweep, 3D coordinates are derived from range and angle estimates; sequences over a 64-length window feed the GRU for trajectory prediction.

Table II
TRAJECTORY PREDICTION METRICS FOR DIFFERENT UAVS

ID	UAV1	UAV2	UAV3	UAV4	UAV5
MAE	0.017	0.006	0.022	0.009	0.112
RMSE	0.176	0.007	0.026	0.013	0.130

Table II reports the mean absolute error (MAE) and root mean square error (RMSE) for five simulated UAV trajectories with varying initial velocities and acceleration profiles. The GRU model consistently captures both linear position progression and subtle curvature induced by acceleration. UAV2, highlighted in the table and visualized in Fig. 8, achieves the best performance and demonstrate the model's ability to accurately predict smooth, accelerated trajectories. Across all trajectories, the GRU model achieves a training RMSE of **0.0663** and a validation RMSE of **0.1363**, indicating strong generalization across diverse motion regimes. The slightly higher error for UAV5 reflects more aggressive maneuvers, however, remains within acceptable bounds for beam steering. These results confirm the effectiveness of GRU-based modeling for UAV trajectory prediction in RIS-assisted ISAC systems, enabling the Near-RT RIC xApp to proactively adapt RIS configurations and maintain continuous tracking through state transitions.

VI. CONCLUSION

This paper presents a ISAC framework with RIS and O-RAN assisted for UAV detection in the CBRS band. It integrates RIS-enhanced sensing, GRU-based trajectory prediction, and O-RAN coordination. The system scales, responds with low latency, and adapts under dynamic spectrum sharing. The sensing pipeline is hierarchical and state driven. It moves smoothly from wide-area scanning to focused tracking. Joint resource management keeps the system responsive to diverse UAV behaviors. Experiments show robust performance and real-time potential across varied trajectories. To strengthen airspace security over cities and critical infrastructure, we will validate on real UAV flight datasets and conduct field trials on a production O-RAN testbed. We will extend to multi-UAV scenarios with cooperative RIS nodes and online-learning xApps, targeting robust NLoS sensing, stable CBRS coexistence, and scalable deployment across dense urban corridors.

ACKNOWLEDGMENT

This material is based upon work supported by the National Science Foundation under Grant Nos. CNS-2431547, OAC-2417890, and OAC-2417891.

REFERENCES

[1] U. Seidaliyeva, L. Ilipbayeva, Kyrmyzy Taissariyeva, Nurzhigit Smailov, and Eric T. Matson. Advances and challenges in drone detection and classification techniques: A state-of-the-art review. *Sensors (Basel, Switzerland)*, 24, 2023. doi: 10.3390/s24010125.

[2] Jurijs Sadovskis and A. Aboltins. Modern methods for uav detection, classification, and tracking. *2022 IEEE 63th International Scientific Conference on Power and Electrical Engineering of Riga Technical University (RTUCON)*, pages 1–7, 2022. doi: 10.1109/RTUCON56726.2022.9978860.

[3] Pietro Casabianca and Yu Zhang. Acoustic-based uav detection using late fusion of deep neural networks. *Drones*, 2021. doi: 10.3390/drones5030054.

[4] Z. Uddin, M. Altaf, M. Bilal, Lewis Nkenyereye, and A. Bashir. Amateur drones detection: A machine learning approach utilizing the acoustic signals in the presence of strong interference. *ArXiv*, abs/2003.01519, 2020. doi: 10.1016/j.comcom.2020.02.065.

[5] Brendan Harvey and Siu O'Young. Acoustic detection of a fixed-wing uav. *Drones*, 2(1), 2018. ISSN 2504-446X. doi: 10.3390/drones2010004.

[6] Paweł Zimroz, P. Trybała, Adam Wróblewski, Mateusz Góralczyk, J. Szrek, Agnieszka Wójcik, and R. Zimroz. Application of uav in search and rescue actions in underground mine—a specific sound detection in noisy acoustic signal. *Energies*, 2021. doi: 10.3390/en14133725.

[7] Diana Tejera-Berengué, Fangfang Zhu-Zhou, M. Utrilla-Manso, R. Gil-Pita, and M. Rosa-Zurera. Acoustic-based detection of uavs using machine learning: Analysis of distance and environmental effects. *2023 IEEE Sensors Applications Symposium (SAS)*, pages 1–6, 2023. doi: 10.1109/SAS58821.2023.10254127.

[8] Jie Zhao, Jingshu Zhang, Dongdong Li, and D. Wang. Vision-based anti-uav detection and tracking. *IEEE Transactions on Intelligent Transportation Systems*, 23:25323–25334, 2022. doi: 10.1109/TITS.2022.3177627.

[9] Chunjuan Bo, Yuntao Wei, Xiujia Wang, Zhan Shi, and Ying Xiao. Vision-based anti-uav detection based on yolov7-gs in complex backgrounds. *Drones*, 2024. doi: 10.3390/drones8070331.

[10] Ziyi Liu, Pei An, You Yang, Shaohua Qiu, Qiong Liu, and Xinghua Xu. Vision-based drone detection in complex environments: A survey. *Drones*, 2024. doi: 10.3390/drones8110643.

[11] Adnan Munir and Abdul Jabbar Siddiqui. Vision-based uav detection in complex backgrounds and rainy conditions. *2024 2nd International*

Conference on Disruptive Technologies (ICDT), pages 1097–1102, 2024. doi: 10.1109/ICDT61202.2024.10489147.

[12] R. Opromolla, G. Fasano, and D. Accardo. A vision-based approach to uav detection and tracking in cooperative applications. *Sensors (Basel, Switzerland)*, 18, 2018. doi: 10.3390/s18103391.

[13] Bingsheng Wei and Martin Barczyk. Experimental evaluation of computer vision and machine learning-based uav detection and ranging. *Drones*, 2021. doi: 10.3390/DRONES5020037.

[14] Yash Vasant Ahirrao, R. Yadav, and Sunil Kumar. Rf-based uav detection and identification enhanced by machine learning approach. *IEEE Access*, 12:177735–177745, 2024. doi: 10.1109/ACCESS.2024.3502754.

[15] Ibrahim Nemer, Tarek Sheltami, Irfan Ahmad, Ansar Ul-Haque Yasar, and Mohammad AR Abdeen. Rf-based uav detection and identification using hierarchical learning approach. *Sensors*, 21(6):1947, 2021.

[16] Florin-Lucian Chiper, Alexandru Marţian, C. Vlădeanu, I. Marghescu, Razvan Craciunescu, and O. Fratu. Drone detection and defense systems: Survey and a software-defined radio-based solution. *Sensors (Basel, Switzerland)*, 22, 2022. doi: 10.3390/s22041453.

[17] Alexandru Marţian, Florin-Lucian Chiper, Razvan Craciunescu, C. Vlădeanu, O. Fratu, and I. Marghescu. Rf based uav detection and defense systems: Survey and a novel solution. *2021 IEEE International Black Sea Conference on Communications and Networking (BlackSeaCom)*, pages 1–4, 2021. doi: 10.1109/BlackSeaCom52164.2021.9527871.

[18] Y. Xie, Ping Jiang, Yi Gu, and Xiao Xiao. Dual-source detection and identification system based on uav radio frequency signal. *IEEE Transactions on Instrumentation and Measurement*, 70:1–15, 2021. doi: 10.1109/TIM.2021.3103565.

[19] Yuan He, Jia Zhang, Rui Xi, Xin Na, Yimiao Sun, and Beibei Li. Detection and identification of non-cooperative uav using a cots mmwave radar. *ACM Transactions on Sensor Networks*, 20:1 – 22, 2024. doi: 10.1145/3638767.

[20] A. De Maio, Jibin Zheng, T. Su, V. Carotenuto, and A. Aubry. An adaptive radar signal processor for uavs detection with super-resolution capabilities. *IEEE Sensors Journal*, 21:20778–20787, 2021. doi: 10.1109/jsen.2021.3093779.

[21] Chenxing Wang, Jiangmin Tian, Jiuwen Cao, and Xiaohong Wang. Deep learning-based uav detection in pulse-doppler radar. *IEEE Transactions on Geoscience and Remote Sensing*, PP:1–12, 2021. doi: 10.1109/TGRS.2021.3104907.

[22] Yuan Wei, Tao Hong, and Chaoqun Fang. Research on information fusion of computer vision and radar signals in uav target identification. *Discrete Dynamics in Nature and Society*, 2022. doi: 10.1155/2022/3898277.

[23] Alan Frid, Y. Ben-Shimol, E. Manor, and S. Greenberg. Drones detection using a fusion of rf and acoustic features and deep neural networks. *Sensors (Basel, Switzerland)*, 24, 2024. doi: 10.3390/s24082427.

[24] Yiyao Wan, Jiahuan Ji, Fuhui Zhou, Qihui Wu, and Tony Q. S. Quek. Vision-radar fusion-based dynamic sparse intrusion uav detection for low-air security. In *2024 16th International Conference on Wireless Communications and Signal Processing (WCSP)*, pages 560–565, 2024. doi: 10.1109/WCSP62071.2024.10827393.

[25] Cunhua Pan, Gui Zhou, Kangda Zhi, Sheng Hong, Tuo Wu, Yijin Pan, Hong Ren, Marco Di Renzo, A Lee Swindlehurst, Rui Zhang, et al. An overview of signal processing techniques for ris/irs-aided wireless systems. *IEEE Journal of Selected Topics in Signal Processing*, 16(5):883–917, 2022.

[26] Huayang Chen, Yechao Bai, Qiong Wang, Hao Chen, Lan Tang, and Ping Han. Doa estimation assisted by reconfigurable intelligent surfaces. *IEEE Sensors Journal*, 23:13433–13442, 2023. doi: 10.1109/JSEN.2023.3273862.

[27] K. B. Serge Angelo Dapa, Guillaume Point, Saleh Bensator, and Fouzia Elbahhar Boukour. Vehicular communications over ofdm radar sensing in the 77 ghz mmwave band. *IEEE Access*, 11:4821–4829, 2023. doi: 10.1109/ACCESS.2023.3235199.

[28] K. B. Serge Angelo Dapa, Fouzia Elbahhar Boukour, Guillaume Point, and Saleh Bensator. Parametrizations of a 77 ghz ofdm joint radar communication. *IEEE Access*, 13:153140–153148, 2025. doi: 10.1109/ACCESS.2025.3596870.

[29] Xiaochan Xue, Saurabh Parkar, Shucheng Yu, and Yao Zheng. Ai-assisted composite isac for mmwave respiration pattern recognition. In *Proceedings of the IEEE Annual Congress on Artificial Intelligence of Things (AIoT)*, page Art. no. 1762147323265. IEEE, December 2025. to appear.

[30] Fan Liu, Yuanhao Cui, Christos Masouros, Jie Xu, Tony Xiao Han, Yonina C. Eldar, and Stefano Buzzi. Integrated sensing and communications: Toward dual-functional wireless networks for 6g and beyond. *IEEE Journal on Selected Areas in Communications*, 40(6):1728–1767, 2022. doi: 10.1109/JSAC.2022.3156632.

[31] Nhan Thanh Nguyen, Quang-Doanh Vu, Kyungchun Lee, and Markku Juntti. Hybrid relay-reflecting intelligent surface-assisted wireless communications. *IEEE Transactions on Vehicular Technology*, 71(6):6228–6244, 2022. doi: 10.1109/TVT.2022.3158686.

[32] Yifei Yuan, Dan Wu, Yuhong Huang, and Chih-Lin I. Reconfigurable intelligent surface (ris) relay: Lessons of past and strategies for its success. *IEEE Communications Magazine*, PP:1–7, 12 2022. doi: 10.1109/MCOM.003.2200193.

[33] Lijie Wu, Qun Yan Zhou, Jun Yan Dai, Siran Wang, Junwei Zhang, Zhen Jie Qi, Hanqing Yang, Ruizhe Jiang, Zheng Xing Wang, Huidong Li, Zhen Zhang, Jiang Luo, Qiang Cheng, and Tie Jun Cui. A wideband amplifying and filtering reconfigurable intelligent surface for wireless relay. *Engineering*, 2025. ISSN 2095-8099. doi: https://doi.org/10.1016/j.eng.2025.06.015.

[34] Michele Polese, Leonardo Bonati, Salvatore D'Oro, Stefano Basagni, and Tommaso Melodia. Understanding o-ran: Architecture, interfaces, algorithms, security, and research challenges, 2022.

[35] Salim El Ghalbzouri, Karim Boutiba, Adlen Ksentini, and Mustapha Benjillali. Neural-driven control of ris in 6g networks: A gosimris and xapp-based framework. *IEEE Networking Letters*, 7:1–5, 2025. doi: 10.1109/LNET.2025.3527683.

[36] Ali Fuat Sahin, Onur Salan, Ibrahim Hokelek, and Ali Gorcin. Ris meets o-ran: A practical demonstration of multi-user ris optimization through ric, 2025.

[37] Maria Tsampazi, Michele Polese, Falko Dressler, and Tommaso Melodia. O-ris-ing: Evaluating ris-assisted nextg open ran. *ArXiv*, abs/2502.18753, 2025. doi: 10.48550/arXiv.2502.18753.

[38] Shao-Yu Lien, Chih-Cheng Tseng, Wei-Cheng Hung, Cheng-You Tsai, Ting-Yu Liu, Der-Jiunn Deng, Yuan-Chun Lin, Shih-Cheng Lin, Chia-Chan Chang, and Sheng-Fuh Chang. Open radio access network ric empowered reconfigurable intelligent surface: A physical-layer security perspective. *IEEE Transactions on Industrial Cyber-Physical Systems*, 2:615–625, 2024. doi: 10.1109/TICPS.2024.3484372.

[39] Bouziane Brik, Karim Boutiba, and A. Ksentini. Deep learning for b5g open radio access network: Evolution, survey, case studies, and challenges. *IEEE Open Journal of the Communications Society*, 3:228–250, 2022. doi: 10.1109/ojcoms.2022.3146618.

[40] Simona Marinova and Alberto Leon-Garcia. Intelligent o-ran beyond 5g: Architecture, use cases, challenges, and opportunities. *IEEE Access*, 12:27088–27114, 2024. doi: 10.1109/ACCESS.2024.3367289.

[41] E.F. Knott, J.F. Schaeffer, and M.T. Tulley. *Radar Cross Section*. Radar, Sonar and Navigation Series. Institution of Engineering and Technology, 2004. ISBN 9781891121258.

[42] Chin-Che Tsai, Cheng-Tai Chiang, and Wen-Jiao Liao. Radar cross section measurement of unmanned aerial vehicles. In *2016 IEEE International Workshop on Electromagnetics: Applications and Student Innovation Competition (iWEM)*, pages 1–3, 2016. doi: 10.1109/iWEM.2016.7504915.

[43] Jan Farlik, Miroslav Kratky, Josef Casar, and Vadim Stary. Radar cross section and detection of small unmanned aerial vehicles. In *2016 17th International Conference on Mechatronics - Mechatronika (ME)*, pages 1–7, 2016.

[44] Ioannis K. Kapoulas, Antonios Hatziefremidis, A. K. Baldoukas, Evangelos S. Valamontes, and J. C. Statharas. Small fixed-wing uav radar cross-section signature investigation and detection and classification of distance estimation using realistic parameters of a commercial anti-drone system. *Drones*, 7(1), 2023. ISSN 2504-446X. doi: 10.3390/drones7010039.

[45] Abigael Taylor and Dominique Poullin. Experimental uav detection using 4g-lte-based passive radar. In *2023 IEEE International Radar Conference (RADAR)*, pages 1–6, 2023. doi: 10.1109/RADAR54928.2023.10371153.

[46] Sirish Deshmukh and K J Vinoy. Design and development of radar for detection of drones and uavs. In *2022 IEEE Microwaves, Antennas, and Propagation Conference (MAPCON)*, pages 1714–1719, 2022. doi: 10.1109/MAPCON56011.2022.10047163.

[47] Zhibo Tang, He Ma, Youmin Qu, and Xingpeng Mao. Uav detection with passive radar: Algorithms, applications, and challenges. *Drones*, 9 (1), 2025. ISSN 2504-446X. doi: 10.3390/drones9010076.